

Observation of soft X-ray Cherenkov radiation in Be and Si foils

S. R. Uglov,¹ A.V.Vukolov

*Tomsk Polytechnic University,
Lenin Avenue 30, Tomsk 634050, Russia*

E-mail: uglov@tpu.ru

ABSTRACT: Currently, most of the Cherenkov phenomenon researches for the X-ray region are theoretical studies; there are only a few experiments in this area. Here the new experimental results on observation of X-ray Cherenkov radiation generated by 5.7 MeV electrons in the thin Be and Si foils are presented. The Cherenkov effect from Be was observed for the first time. The experimental results are compared with the calculations performed according to the theoretical model of transition radiation taking into account the oxide layer on the target output surface.

KEYWORDS: Cherenkov and transition radiation; X-ray generators and sources; Interaction of radiation with matter.

¹Corresponding author.

Contents

1	Introduction	1
2	Spectral and angular properties of XCR	2
3	Method and setup	5
4	Results and discussion	8
5	Conclusion	11

1 Introduction

It is known that the Cherenkov radiation (CR) is generated by a charged particle moving in a medium with a refraction index $n > 1$, if the particle velocity $\beta = v/c > 1/n$. The Cherenkov radiation in the optical range is widely known and is used, for example, in charged particle detectors. Also for some substances, the condition $n > 1$ is met at small spectrum intervals in the region of vacuum ultraviolet [1, 2] and soft X-rays near the radiation absorption edges [3–8]. So the Cherenkov radiation for X-ray (XCR) is possible too. This radiation is considered as an effective method of obtaining radiation in the ultrasoft X-ray range [8–10], including in the region of the "water window" ($E = 280 \div 543$ eV) [8, 9] and "carbon window" ($E = 248 \div 282$ eV), which are relevant in biological research [11].

Currently, most of the XCR researches are theoretical studies [12–17], and there are only a few experiments in this area. These experiments presented convincing experimental evidence for the observation of the Cherenkov effect in the X-ray range. At the same time, not all experimental results show complete agreement with the theory.

Thus, after the first experimental observation of the Cherenkov effect in the ultra-soft X-ray range near the K-edge of carbon absorption [3], Dutch researchers obtained in their study [6] an experimental confirmation of the Cherenkov effect existing near the absorption edges of elements such as titanium, vanadium, and silicon; at the same time, they failed to detect the Cherenkov effect for Ni and to confirm the Cherenkov effect in carbon [9]. The carbon-related researches were carried out using various modifications of carbon such as diamond, amorphous carbon, graphite and carbon in organic compounds using a lower electron energy than in [3], but sufficient for the appearance of Cherenkov radiation according to the theory.

There are also disagreements between the calculations of the XCR angular density and the experimental observation of the one during the sliding interaction of 75 MeV electron beam with targets [10]. For example, the experimental Cherenkov angles for carbon and Si turned out to be the same, which does not agree with the theory.

Among the recent experimental studies, the results that was observed on the inner electron beam of the special synchrotron "MIRRORCLE-20" [19] are of particular interest. In this experimental studies, an anomalously high angular density of soft X-ray radiation was observed in the plane perpendicular to the magnetic field of the synchrotron. This effect still has no convincing explanation.

The above-mentioned discrepancies of some experimental results with the theory and the fewness of experimental studies are the motive to new experimental studies of XCR, for example, to take the test on ability the other substances to generate the XCR. So recently we have demonstrated the observation of XCR near the L-edge of Al which was generated by 5.7 MeV electrons [20].

In this paper, we present new results of observation and research of the XCR for the following two substances: 1) thin Be foil: a next new chemical element in which the observation of XCR is expected; 2) thin Si target foil was used as the control for which experimental confirmation of the XCR existence has been obtained previously [6]. The obtained experimental results were compared to the calculations performed using the study by Pafomov [21].

2 Spectral and angular properties of XCR

The fundamental possibility of observing the XCR effect in some substance can be determined based on the properties of its dielectric constant $\epsilon(\omega)$

$$\epsilon(\omega) = 1 + \chi'(\omega) + \chi''(\omega), \quad (2.1)$$

where $\chi'(\omega)$ and $\chi''(\omega)$ are real and imaginary parts of the dielectric susceptibility. The Cherenkov effect can appear for this substance, if the parameter $\chi'(\omega) > 0$. As $\epsilon(\omega) = n(\omega)^2$ ($n(\omega)$ is the refraction index), then, considering that for the X-ray range $n(\omega) \sim 1$ and, therefore, $\chi'(\omega) \ll 1$ and $\chi''(\omega) \ll 1$, the condition, that corresponds to the main appearance condition of the Cherenkov radiation for the target material $n(\omega) > 1$, shall be $\chi' > 0$. This condition, for example, for Be, Al, and Si atoms, is met near the corresponding K and L edges of the radiation absorption by matter.

Figure 1 shows the values of $\chi'(\omega)$ and $\chi''(\omega)$ for Be, Al, and Si, as calculated using the data of [18]. The second condition for the XCR appearance is the required velocity of a charged particle v , that is derived from the condition $\beta = v/c > 1/n$ or $\chi'(\omega) \geq \gamma^{-2}$, where γ is the Lorentz factor of the charged particle. The velocity value v with $\gamma^{-2} = \chi'(\omega)$ determines the energy threshold of the Cherenkov effect appearance. In figure 1, the dash line marks the value γ^{-2} for electrons with energy of 5.7 MeV.

The Cherenkov effect for substances shown in figure 1 should appear in the spectral ranges of photon energies between intersection points of the corresponding $\chi'(\omega)$ with the dash line γ^{-2} . However, because of radiation self-absorption by the target substance, due to a sharp increase in absorption near the K or L edge, the actual observation range of the Cherenkov effect on the right side of the spectrum is limited by the energy value corresponding to the absorption edge E_S . Therefore, the Cherenkov effect can be actually observed only in the energy interval corresponding to the left slope of the curve $\chi'(\omega)$.

In theoretical models of transition radiation, the Cherenkov effect appears automatically when the condition $\cos(\theta_{ch}) = 1/\beta n(\omega)$ is satisfied for photon energy $E = \hbar\omega$ and radiation angle θ . When

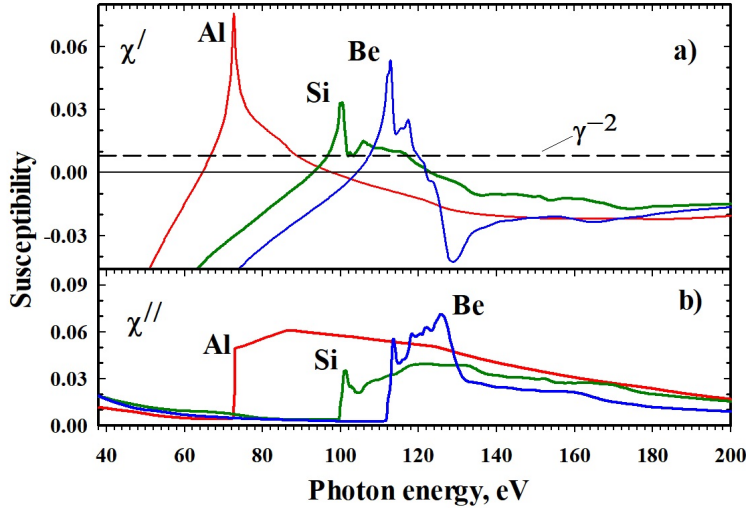


Figure 1. Solid lines are $\chi'(\omega)$ (a) and $\chi''(\omega)$ (b) for Be, Al, and Si, as calculated using the data of [18]. Dashed line is γ^{-2} for electron energy $E_e = 5.7$ MeV.

this condition is satisfied, a sharp peak in the spectrum of radiation emitted at the corresponding angle θ_{ch} appears against the background of the “white” transition radiation spectrum.

The theoretically expected spectrum and distribution of the angular density of the XCR, including the transition radiation generated in the vicinity of the Cherenkov radiation, have been calculated using the formulas from [21] in the semi-infinite target approximation.

Thus, figure 2 shows full radiation spectra for Al, Si and Be integrated over the entire radiation cone in the forward direction for electrons with a total energy of $E = 5.7$ MeV.

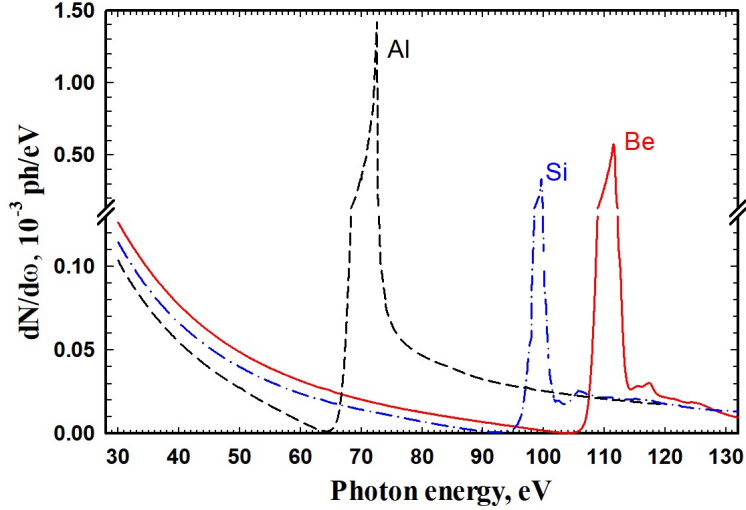


Figure 2. Radiation spectra for Al, Si, and Be targets was calculated using [21] for the transition radiation forward from a semi-infinite target for a (total) electron energy of $E_e = 5.7$ MeV

The figure 3 shows the spectral-angular radiation densities for Al, Si and Be, calculated along

the radiation plane for the range when the conditions $\beta n(\omega) \geq 1$ are satisfied. The 2D patterns illustrate the general properties of XCR such as the energy range and the line width of the spectrum of the XCR photons, the angular width of the XCR cone and the structure of the XCR intensity distribution within the cone. The values of $dN/d\omega/d\Omega$ for Be, Si and Al are presented using scale factors 1, 2 and 0.7, respectively. The table 1 shows the photon energy E_{max} , the emission angle θ_{max} and the yield corresponding to the maximum spectral-angular density. The E_L and E_R in the table 1, indicate the boundaries of the spectral interval meeting the XCR appearance condition.

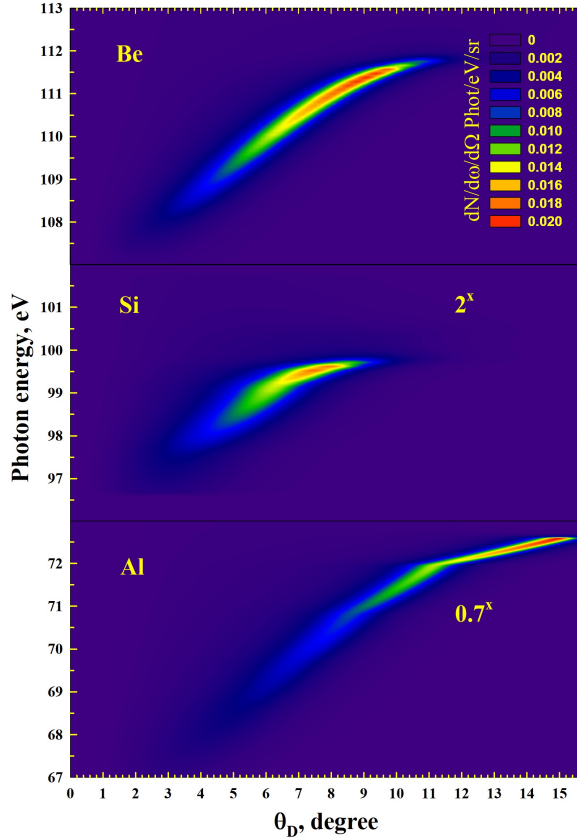


Figure 3. Spectral angular radiation density in the range where the appearance condition is met for the XCR generated along the radiation plane

The calculation results in figure 4 show the angular radiation distributions in the spectral range of $\Delta E = 30 \div 130$ eV as calculated for Al, Be, and Si, both within the photon energy range meeting the Cherenkov condition (dash-dot lines) and being out of this range (dash-double-dot lines), when only the transition radiation is generated.

The solid lines in figure 1 correspond to the angular distribution components as calculated for a series of photon energies within the spectral range with the width of $\Delta E = 1$ eV within the Cherenkov range: $\Delta E_{ch} = E_L \div E_R$. Note that in the provided calculations the radiation generated within the Cherenkov energy range is not a pure Cherenkov radiation, but it has an addition from the transition radiation generated at the target's output surface.

The calculations in figure 3 and 4 show that the total angular distribution of the transition

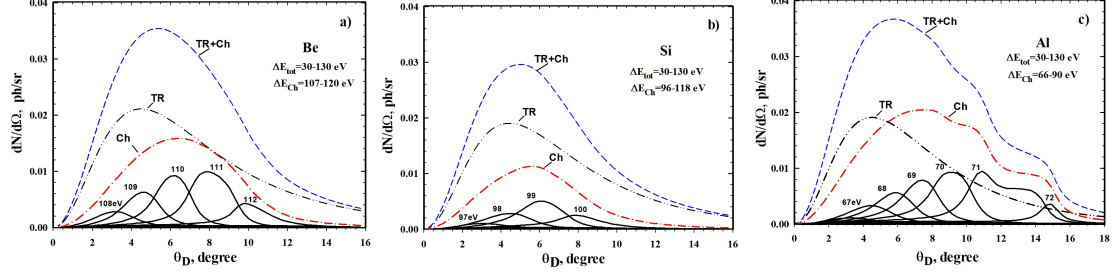


Figure 4. Components of the angular distribution of the Cherenkov (Ch) and transition (TR) radiations for Be (a), Si (b), and Al (c) depending on the photon energy. Solid lines are calculated for $\Delta E = 1$ eV; the dash-dot line is the contribution of Ch; the dash-double-dott line is the contribution of TR outside the Cherenkov interval; the dotted line is TR+Ch within the range of $E = 30 \div 130$ eV.

and Cherenkov radiations has no pronounced narrow “Cherenkov cone” that is characteristic of the Cherenkov radiation within the optical range [22]. The value of θ_{max} corresponding to the maximum of the spectral-angular density of XCR is different from the value of Θ_{max} – the maximum radiation of the angular density $dN/d\Omega$ (see table 1 columns 6 and 9). The angular distributions of the transition radiation generated over the entire spectral interval under consideration and that of XCR virtually coincide both in intensity and in the emission direction (see table 1). Therefore, the calculations of spectra and angular distributions show that it is difficult to experimentally prove the Cherenkov effect in the X-Ray range based on the analysis of the angular distribution shape. A more convincing result can be obtained by spectral research, by finding an intense spectral line in the spectrum of radiation emitted in the direction of the expected Cherenkov radiation cone, with the energy virtually coinciding with the energy of the corresponding absorption edge.

Table 1. Spectral and angular properties of XCR and TR

XCR spectral range with $E_e = 5.7$ (MeV)			Cherenkov radiation						Transition radiation, $\Delta E = 30 \div 130$ (eV)	
1	2	3	4	5	6	7	8	9	10	11
E_L (eV)	E_R (eV)	E_S (eV)	$dN/d\omega/d\Omega$ (ph/sr/eV)	θ_{max} (degr)	E_{max} (eV)	$dN/d\Omega$ (ph/sr)	Θ_{max} (deg)	$dN/d\Omega$ (ph/sr)	θ_{max} (deg)	
Al	66.7	89.5	72.6	0.0287	14.63	72.52	0.0205	7.6	0.0191	4.44
Si	96.6	117.5	99.8	0.0091	7.5	99.52	0.0113	5.75	0.0190	4.38
Be	107.4	120.1	111.5	0.0201	8.75	111.29	0.0159	6.25	0.0211	4.5

3 Method and setup

In the research of the radiation spectral composition, we used the Bragg scattering of radiation by a multilayer mirror. Figure 5a shows the XCR observation setup using the Bragg reflection of a radiation cone fragment near the angle θ_{Ch} using a multilayer mirror $[Mo/B_4C]^{100}$ with a period $d = 7.56$ nm to select the radiation by photon energy.

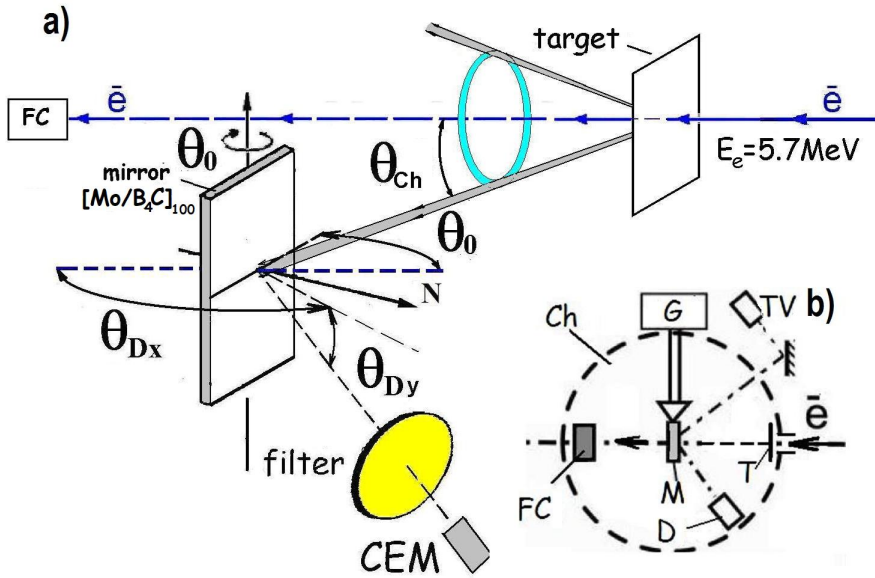


Figure 5. a) Scheme for XCR investigation using a multilayer mirror; b) top view of the vacuum chamber - Ch; T is a target, D is a channel-electron multiplier (CEM), M is a multilayer mirror, G is a goniometer, FC is a Faraday cup.

The results of calculations of the radiation intensity reflected by a multilayer mirror, depending on the angle θ_0 , are shown in figure 6. The calculations have been performed for radiation emitted along the radiation plane coinciding with the mirror rotation axis θ_0 . The calculations have taken into account the reflection index of the multilayer mirror as calculated using [23–25] by the recurrence relation method for the spectral-angular density of the transition and Cherenkov radiations calculated according to [21] for the spectral interval $\Delta E = 30 \div 400$ eV.

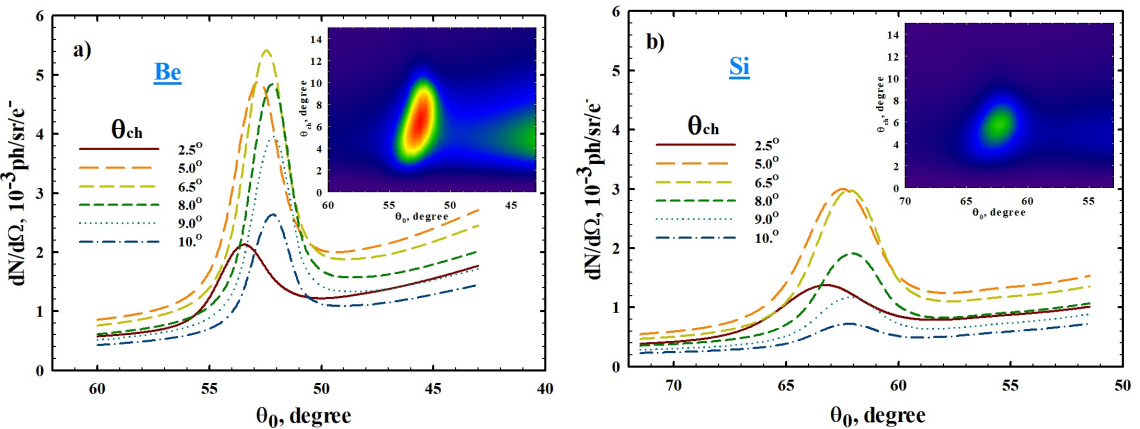


Figure 6. Intensity of radiation reflected by a multilayer mirror $[\text{Mo}/\text{B}_4\text{C}]^{100}$ depending on θ_0 : a) for Be and b) for Si targets.

The maximum values on the curves correspond to the XCR photon energy. For a target that generates only transition radiation, for example, for a Mylar film [20], no maximum should be

observed. The experiment was carried out on a 5.7 MeV electron beam extracted from the M-5 microtron of the Tomsk Polytechnic University [26]. The top view of the scattering chamber is shown in figure 5b. The accelerator operating frequency was 50 Hz; the duration of the macro impulse of the extracted electron beam (MIB) was $0.4 \mu\text{s}$. In the scattering chamber, the beam had a circle shape with $\varnothing = 2 \div 3 \text{ mm}$. The average number of accelerated electrons, as measured using a Faraday cup installed behind the target, was 2.5×10^7 per MIB.

The targets were located at the entrance to the scattering chamber. In both cases, the target thickness was much greater than the length of the radiation absorption by the target at the Cherenkov radiation energy. The beryllium target had the thickness of $t_{Be} = 26 \mu\text{m}$; the silicon target, $t_{Si} = 4 \mu\text{m}$. The transverse dimensions of the targets were $20 \times 20 \text{ mm}$ and $6 \times 8 \text{ mm}$, respectively.

In the center of the scattering chamber, at the distance of $t_m = 200 \text{ mm}$ from the target, there was a multilayer mirror installed. The mirror working size was formed using a special mask made of Mylar with rectangular vertical diaphragm $10 \times 35 \text{ mm}^2$ in size, installed directly on the mirror body. The mirror $[\text{Mo}/\text{B}_4\text{C}]^{100}$ consisted of 100 pairs of Mo and B_4C layers on a silicon substrate. The mirror period was $d = 7.56 \text{ nm}$; the ratio of the B_4C layer thickness to the mirror period was $\Gamma = 0.5$. The composition of the transition layers was estimated as consisting of a mixture of $5\text{Mo} + \text{B}_4\text{C}$ with a thickness of $\Delta t = 0.9 \div 0.95 \text{ nm}$. On average, the mirror reflection index, as calculated using the IMD-5 [27] package in the specular scattering approximation, was $30 \div 35 \%$ in the photon energy interval $\Delta E = 80 \div 120 \text{ eV}$.

The rotation axis of the multilayer mirror crossed the electron beam axis at a right angle. The mirror upper edge was 20 mm below the electron beam axis.

The radiation reflected by the multilayer system was recorded by a spiral channel electron multiplier (CEM) with a funnel (make: SEM-6). The CEM operated in the counting mode, keeping the linearity at loading up to 2 pulses per MIB. The CEM loading was monitored per 100 MIB of the accelerator and, generally, was 10 to 20 pulses per 100 MIB.

The detector recording efficiency, as averaged over an entrance window 9 mm in diameter, was 6.9 % at the photon energy of 96.7 eV and 6.5 % at the photon energy of 77.1 eV. The lower threshold of the detector is about $E_{low} = 5 \text{ eV}$ [28–30].

The detector was at the distance of $L_D = 144 \text{ mm}$ from the mirror. Between the detector and the mirror, we installed a block of permanent magnets to protect the detector from scattered electrons and a nitrocellulose (NC) plastic filter with a thickness of about $0.2 \mu\text{m}$ to suppress the soft component $\hbar\omega < 50 \text{ eV}$ of the transition radiation. To eliminate the effect of scattered magnetic fields on the electron beam, the permanent rare-earth magnets were installed inside a steel case (SC). The SC was placed at 50 mm from target, had length along the radiation registration direction of 80 mm and had the through hole of $\varnothing = 15 \text{ mm}$, that served as a preliminary collimator. The strength of magnetic-field within SC was about $H = 0.1 \text{ T}$. The radiation from the mirror was additionally collimated by two slits with widths of 7 mm and 8 mm that placed in the center and at the out hole of the SC, respectively.

The axis of the radiation registration channel between the mirror and the detector is formed by the diaphragms in the direction of mirror reflection of the fragment of the cone radiation corresponding to $\theta_{Ch} = 6.5^\circ$. The angular sizes and solid angle of the radiation cone fragment registered by the detector were $\Delta\theta_{Ch}^x = \pm 0.67^\circ$, $\Delta\theta_{Ch}^y = \pm 0.74^\circ$ and $\Omega = 5.2 \times 10^{-4} \text{ sr}$, respectively. The detector rotation axis coincided with the mirror rotation axis.

Figure 7 shows the expected intensity of the radiation reflected by the multilayer mirror $[\text{Mo}/\text{B}_4\text{C}]^{100}$ for Be and Si targets as a function of the inclination angle θ_0 at $\theta_{Ch} = 6.5^\circ$.

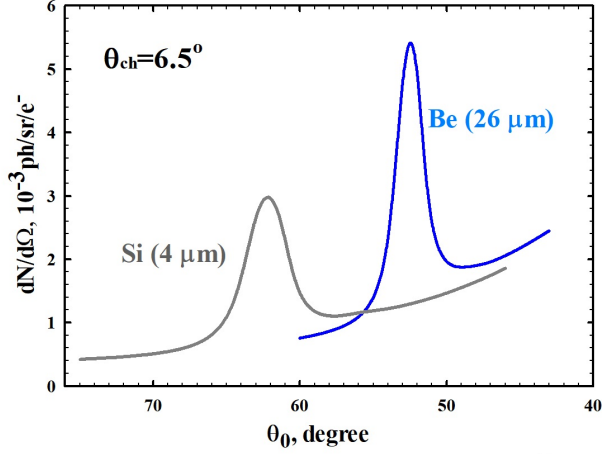


Figure 7. Intensity of the reflected radiation as a function of the angle θ_0 of the $[\text{Mo}/\text{B}_4\text{C}]^{100}$ mirror for Si and Be targets; $\theta_{Dy} = 6.5^\circ$.

4 Results and discussion

The intensity of the radiation reflected by the multilayer mirror in the Bragg direction was found for each θ_0 from the results of the initial measurement of the radiation intensity as a depending on the observation angle θ_{Dx} . The maximum values of the measured angular distributions after subtracting the background were used for plotting the intensity of the reflected radiation vs θ_0 . Figure 8 shows

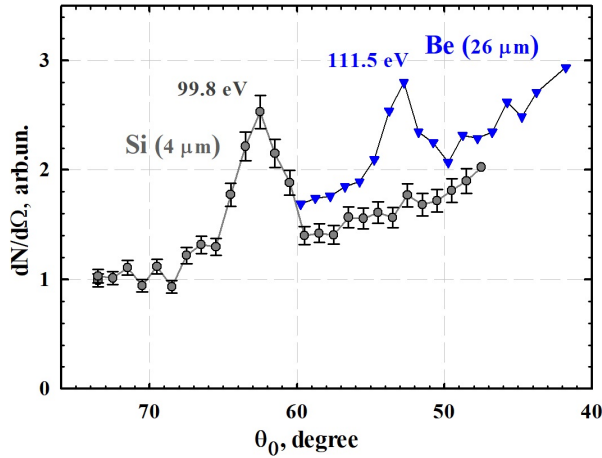


Figure 8. Intensity of the reflected radiation as a function of the angle θ_0 of the $[\text{Mo}/\text{B}_4\text{C}]^{100}$ mirror for Si (grey circles) and Be (blue triangles) targets; $\theta_{Dy} = 6.5^\circ$.

the maximum intensity values of the radiation reflected by the mirror as obtained for Si and Be targets. As one can see, the general view and position of the maxima of the experimental curves

are similar to the curves in figure 7. The maximum values on the curves at angles of $\theta_0 = 62^\circ$ and $\theta_0 = 52^\circ$ correspond to the energy $E_{Si} = 99.8$ eV (the bottom curve) and $E_{Be} = 111.5$ eV (the upper curve). The values E_{Si} and E_{Be} are quite consistent with the L and K absorption edges of silicon and beryllium, respectively. Therefore, we can affirm that we experimentally observed the X-ray Cherenkov radiation for the first time in a target made of Be and confirmed the X-ray Cherenkov radiation in Si. However, when comparing the results in detail, we see a discrepancy between the relative intensities as predicted by calculations.

We consider that one of the main reasons for such difference between theory and experiment is the presence of the oxide layer or another contamination on the target surface. To take into account for the effect of an additional layer, we carried out calculations using Pafomov's expressions for a target consisting of three substances. It's semi-infinite metal/oxide/vacuum in our case. Expressions have complicated view and one may find them in [21]. The calculations were carried out using a homogeneous layer of BeO or SiO_2 oxides as an additional layer on the target surface. The results of calculating the effect of the oxide film on the total radiation spectrum using beryllium as an example are shown in figure 9. Calculations have been performed for a 180 nm thick homogeneous oxide layer.

In calculations for BeO, we took into account the chemical shift which leads to a shift of the beryllium absorption edge in combination with oxygen by 2.8 eV towards a higher energy [31–33]. The chemical shift of the absorption edge in SiO_2 is 4.5 eV. As can be seen in figure 9, the effect of the oxide layer on the emission spectrum manifests itself in the suppression of Cherenkov radiation and in the increase of the transition radiation.

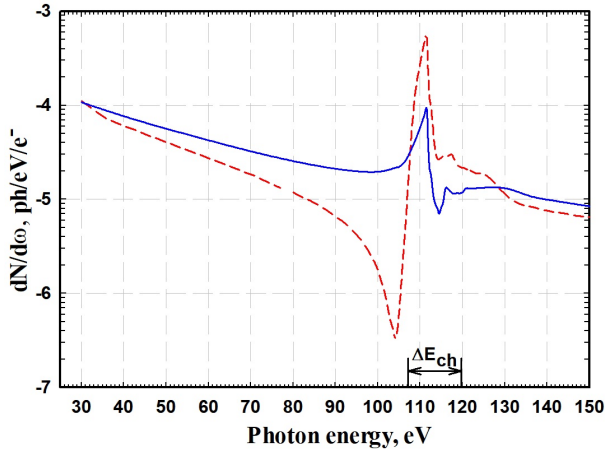


Figure 9. Radiation spectra for: dash line - Be target; solid line - Be targets with a 180 nm thick BeO layer.

Note that in the case of oblique interaction of the electron beam with the target, the suppression of the Cherenkov radiation yield should be expected due to an increase in the effective oxide thickness.

Figure 10 shows the experimental results as compared with the calculation results obtained for a three-component medium according to [21], taking into account the radiation registration efficiency by the detector, the NC filter transparency, the efficiency of radiation reflection by the mirror, and the thickness of the oxide film.

As can be seen from the figure 10, in order to agree the results of the calculation with the experiment, it is necessary to take into account a certain inclined pedestal.

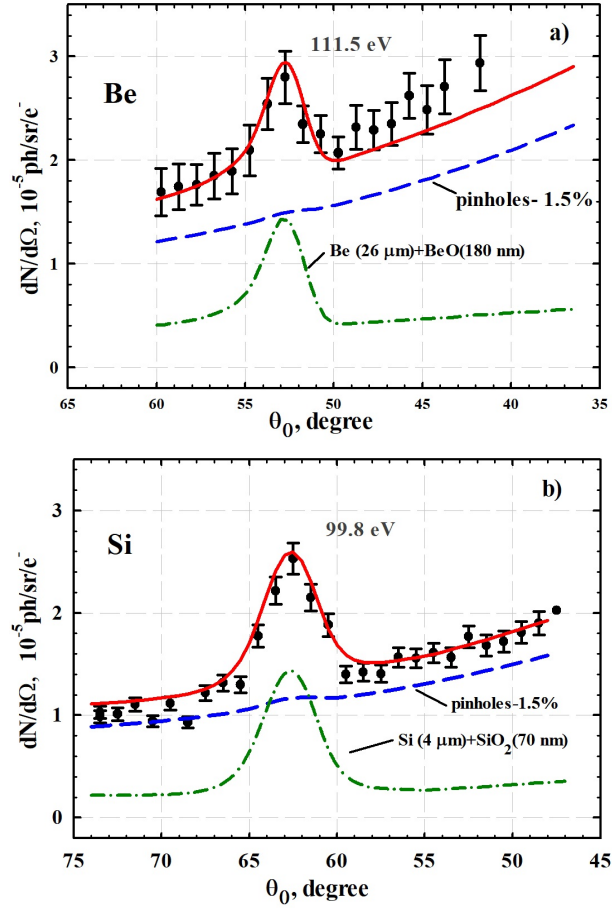


Figure 10. Comparison of calculation and experimental results of the scanning of the radiation spectrum from Be and Si targets by a multilayer mirror.

The simple estimation showed that the pedestal radiation intensity is much higher than the contributions from bremsstrahlung and characteristic radiations. The most plausible explanation for the pedestal is the presence of pinholes in the NC filter. In this case, the high intensity of the pedestal is due to the contribution of the specular reflection of the high-intensity soft part ($E < 50$ eV) of the transition radiation passed through the pinholes in the NC filter. In order to take into account the contribution due to the pinholes, the emission spectra for Be and Si were calculated starting with the photon energy $E = 5$ eV, which is the lower threshold of the detector efficiency. Since for the optical constants in [18] the lower bound of the photon energy is $E = 30$ eV, calculations for photons with energy $E = 5-30$ eV were carried out using the database [34].

The calculation results presented in figure 10 by the solid lines were obtained at an oxide layer thickness of 180 nm and 70 nm for Be and Si, respectively, taking into account that the total pinhole aperture in the NC filter was 1.5% of the total detector aperture. The beam divergence was taken into account as normal distribution with $\theta^2 = 10^{-4}$.

The dashed curve in the figure 10 shows the contribution associated with radiation transmitted through pinholes. The good agreement between the calculation results and the experiment was obtained by selecting the thickness of the oxide layer and the fraction of the radiation transmitted through the pinholes.

To verify the presence of an oxide layer on the target surface, the additional study of the elemental composition of the Be target surface using the radio-frequency glow discharge method (RF-GD-OES) was carried out by “GD- PROFILER-2” which showed the qualitatively confirmed presence of a BeO layer with an average thickness of 0.1 to 0.5 μm on the target surface. The thickness of the oxide layer for a silicon target was not tested.

5 Conclusion

As we showed above, the calculations that include the effect of the oxide layer and pinholes, demonstrate an improvement in the agreement between the calculations and the experiment. However, it should be noted that these calculations were performed using some simplifications and idealization of the parameters of the multilayer mirror and targets. So, for example, the mirror reflectivity was calculated for an ideal periodic structure, the model of the target did not take into account the change of the oxide concentration with increasing distance from the target surface. Besides it's necessary to keep in mind the well-known fact that at low energies of X-ray radiation tabular data for $\text{Re}(\chi)$ and $\text{Im}(\chi)$ have high uncertainties [34, 35].

Yet, despite the inaccuracies of the models of the multilayer mirror and the surface layer of the target, we can conclude that the results of our studies confirm the existence of the Cherenkov effect for Be and Si. And the Cherenkov effect observation in Be has been presented for the first time. The measured radiation intensity is comparable to the theoretically expected value. The fact of observing the Cherenkov radiation in Be may promote the development of a high-intensity, high-monochrome radiation source with the energy of emitted photons $E \sim 111$ eV. Following [13], the spectral-angular radiation density of such a source can be increased several times by using the sliding interaction of the electron beam with the target. Besides, the threshold nature of the XCR can be used for the development of threshold counters for the separation of the charged particles. These detectors are more promising for use with multiply charged ions since the XCR yield is proportional to the square of the particle charge.

Acknowledgments

This work has been supported by the Competitiveness Enhancement Program of the Tomsk Polytechnic University (project-185/2020).

References

- [1] M. A. Piestrup, R. H. Pantell, H. E. Puthoff and G. B. Rothbart, *Čerenkov radiation as a source of ultraviolet radiation*, *J. Appl. Phys.* **44** (1973) 5160.
- [2] M. A. Piestrup, R. A. Powell, G. B. Rothbart, C. K. Chen and R. H. Pantell, *Čerenkov radiation as a light source for the 2000–620-Å spectral range*, *Appl. Phys. Lett* **28** (1976) 92.

- [3] V. A. Bazylev, V. I. Glebov, E. I. Denisov, N. K. Zhevago, A. S. Khlebnikov, V. G. Tsinoev, Yu. P. Chertov, B. I. Shramenko, *Observation of Čerenkov radiation with a photon energy of 284 eV*, *JETP Letters* **34** (1981), 97.
- [4] V. A. Bazylev, V. I. Glebov, E. I. Denisov, N. K. Zhevago, M. A. Kumakhov, A. S. Khlebnikov and V. G. Tsinoev, *X-ray Čerenkov radiation. Theory and experiment*, *Sov. Phys. – JETP* **54** (1981) 884.
- [5] V. A. Bazylev, V. I. Glebov, E. I. Denisov, N. K. Zhevago, A. S. Khlebnikov, *Čerenkov radiation as an intense x-ray source*, *JETP Lett.* **24** (1976) 371.
- [6] W. Knulst, van der M. J. Wiel, O. J. Luiten and J. Verhoeven, *Observation of narrow-band Si L-edge Čerenkov radiation generated by 5 MeV electrons*, *Appl. Phys. Lett.* **79** (2001) 2999.
- [7] W. Knulst, van der M. J. Wiel, and O. J. Luiten and J. Verhoeven, *High-brightness, narrowband, and compact soft x-ray Cherenkov sources in the water window*, *J., Appl. Phys. Lett.* **83** (2003) 4050.
- [8] W. Knulst, J. Luiten and J. Verhoeven, *Compact, high-brightness soft x-ray Cherenkov sources*, *IEEE J. Sel. Top. Quantum Electron.* **10** (2004) 1414.
- [9] W. Knulst, *PhD Thesis*, Thechnische Universit, Eindhoven (2004).
- [10] M. J. Moran, B. Chang, M. B. Schneider and X. K. Maruyama, *Grazing-incidence Cherenkov X-ray generation*, *Nucl. Instrum. Methods* **B48** (1990) 287.
- [11] I.A. Artyukov, A.V. Vinogradov, Yu.S. Kasyanov, and S. V.Saveliev, *About X-ray microscopy in the “carbon window”*, *Quantum Electronics* **34** (2004) 691.
- [12] V. A. Bazylev and V.I. Glebov, *X-ray Čerenkov radiation at grazing incidence of electrons*, *Physics Letters* **A160** (6) (1991) 564.
- [13] C. Gary, V. Kaplin, A. Kubankin, N. Nasonov, M. Piestrup, S. Uglov, *An investigation of the Čerenkov X-rays from relativistic electrons*, *Nucl. Instrum. Methods Phys. Res. B* **227** (2005) 95.
- [14] A. S. Konkov, P. V. Karataev, A. P. Potylitsyn and A. S. Gogolev, *X-Ray Cherenkov Radiation as a Source for Transverse Size Diagnostics of Ultra-relativistic Electron Beams*, *Journal of Physics: Conference Series* **517** (2014) 012003.
- [15] M. Shevelev, A. Konkov and A. Aryshev, *Soft-x-ray Cherenkov radiation generated by a charged particle moving near a finite-size scree* *Phys. Rev. A* **92** (2015) 052851.
- [16] M. Shevelev, A. Konkov, B. Alekseev, *Spectral and polarization characteristics of X-ray hybrid radiation*, *Nucl. Instrum. Methods Phys. Res. B* **464** (2020) 117.
- [17] M. V. Bulgakova, V. S. Malyshevsky, and G. V. Fomin, *X-Ray Cherenkov Radiation in an Absorbing Medium with Finite Dimensions* *Journal of Surface Investigation. X-Ray, Synchrotron and Neutron Techniques* **14** (2020) 264.
- [18] <http://www.esrf.fr/computing/expg/subgroups/theory/DABAX/dabax.html>
- [19] H. Yamada, D. Minkov, Y. Shimura, C. Scourtis, O. K. Ejike, D. Hasegawa, M. Yamada, T. Hanashima and K. Atkinson, *Measurement of angular distribution of soft X-ray radiation from thin targets in the tabletop storage ring MIRRORCLE-20SX*, *J. Synchrotron Rad.* **18** (2011) 702.
- [20] S. Uglov, A. Vukolov, V. Kaplin, L. Sukhikh and P. Karataev, *Observation of soft X-ray Cherenkov radiation in Al*, *EPL (Europhysics Letters)* **118** (2017) 34002.
- [21] V. E. Pafomov, *Radiation of a charged particle at the interfaces presence*, *Trudy FIAN* **44** (1969) 28.
- [22] J. V. Jelley, *Cherenkov Radiation and Its Applications*, London:Pergamon, (1958).
- [23] L. G. Parratt, *Surface Studies of Solids by Total Reflection of X-Rays*, *Phys. Rev.* **95** (1954) 359.

- [24] A.V. Vinogradov, I.V Kozhevnikov, *Multilayer x-ray mirrors*, *Trudy FIAN* **196** (1989) 62.
- [25] V.G. Kohn, *Towards the theory of specular reflection of X-rays by multilayer mirrors*, *Journal of Surface Investigation. X-Ray, Synchrotron and Neutron Techniques* **1** (2003) 23.
- [26] S. R. Uglov, V. V. Kaplin, A. P. Potylitsyn, L. G. Sukhikh, A. V. Vukolov, G. Kube, *Investigation of the characteristics of EUV backward transition radiation generated by 5.7 MeV electrons in mono- and multilayer targets*, *J. Phys.: Conf. Ser.* **51** (2014) 012009.
- [27] <http://www.esrf.eu/Instrumentation/software/data-analysis/xop2.3>
- [28] M. R. Einbund, B. V. Polenov, *Secondary electron multipliers and their application*, Moscow: Energoatomizdat (1981).
- [29] J. E. Mack, F. Paresce and S. Bowyer, *Channel electron multiplier: its quantum efficiency at soft x-ray and vacuum ultraviolet wavelengths*, *Appl. Optics* **15** (1976) 861.
- [30] A. A. Legkodymov, M. R. Mashkovtsev, A. D. Nikolenko, V. F. Pindyurin, V. V. Lyakh, S. V. Avakyan and N. A. Voronin, *Comparative of Secondary-Electron Multipliers within the Ultrasoft X-ray Range*, *Journal of Surface Investigation. X-Ray, Synchrotron and Neutron* **6** (2012) 404.
- [31] V. I. Nefedov, *Handbook "X-ray Electron Spectroscopy of Chemical Compounds"*, Published by Chemistry, Moscow, "Khimiya" (1984).
- [32] E. D. Palik, *Handbook of Optical Constants of Solids III*, Academic Press, San Diego, CA (1998).
- [33] C.D. Wagner, W. M. Riggs, L. E. Davis, J. F. Moulder and G. E. Muilenberg, *Handbook of x-ray photoelectron spectroscopy*, Published by Perkin-Elmer (1979).
- [34] D. E. Cullen, J. H. Hubbell and L. Kissel, *EPDL97: The Evaluated Photon Data Library '97 Version*, Lawrence Livermore National Laboratory Report UCRL-50400 **6** (1997) 36.
- [35] <https://physics.nist.gov/PhysRefData/FFast/Text2000/sec06.html#tab2>